Commun. Theor. Phys. **72** (2020) 045502 (17pp) https://doi.org/10.1088/1572-9494/ab76ff

Stable Fano-like plasmonic resonance: its impact on the reversal of far- and near-field optical binding force

Hamim Mahmud Rivy[1,2,4], M R C Mahdy[1,3,4], Nabila Masud[1], Ziaur Rahman Jony[1] and Saikat Chandra Das[1]

[1] Department of Electrical & Computer Engineering, North South University, Bashundhara, Dhaka, 1229, Bangladesh
[2] School of Electrical and Electronic Engineering, Nanyang Technological University, 50 Nanyang Ave, 639798 Singapore
[3] Pi Labs Bangladesh LTD, ARA Bhaban, 39, Kazi Nazrul Islam Avenue, Kawran Bazar, Dhaka 1215, Bangladesh

E-mail: mahdy.chowdhury@northsouth.edu

Received 7 November 2019, revised 8 January 2020
Accepted for publication 19 January 2020
Published 30 March 2020

Abstract

Even for a 100 nm interparticle distance or a small change in particle shape, optical Fano-like plasmonic resonance mode usually vanishes completely. It would be remarkable if stable Fano-like resonance could somehow be achieved in distinctly shaped nanoparticles for more than 1 μm interparticle distance, which corresponds to the far electromagnetic field region. If such far-field Fano-like plasmonic resonance can be achieved, controlling the reversal of the far-field binding force can be attained, like the currently reported reversals for near-field cases. In this work, we have proposed an optical set-up to achieve such a robust and stable Fano-like plasmonic resonance, and comparatively studied its remarkable impact on controlling the reversal of near- and far-field optical binding forces. In our proposed set-up, the distinctly shaped plasmonic tetramers are half immersed (i.e. air–benzene) in an inhomogeneous dielectric interface and illuminated by circular polarized light. We have demonstrated significant differences between near- and far-field optical binding forces along with the Lorentz force field, which partially depends on the object's shape. A clear connection is shown between the far-field binding force and the resonant modes, along with a generic mechanism to achieve controllable Fano-like plasmonic resonance and the reversal of the optical binding force in both far- and near-field configurations.

Keywords: Fano resonance, optical binding force, Lorentz force, plasmonic, tetramer

(Some figures may appear in colour only in the online journal)

1. Introduction

Recently, Fano or Fano-like plasmon resonance in hybridized plasmonic nanostructures has become a subject of intense study due to its broad range of applications in surface-enhanced Raman scattering [1], biosensing [2], waveguiding [3] and so on [4]. Despite having a broad range of applications, until now, it has been quite challenging to achieve robust and stable Fano or Fano-like plasmon resonance in plasmonic nanostructures due to its complex nature. This kind of resonance mainly originates from the destructive interference between the bright resonant mode and the dark resonant mode, which has been reported in different aggregations of plasmonic nanoparticles, i.e. monomers, dimers, trimers, tetramers, seven or even larger aggregations [5–9]. In those configurations, Fano-like resonance has shown strong dependency over the interparticle gap, geometry of the structure, particle size, shape, center symmetry and the

[4] Equal contribution.

surrounding medium. Even a small change in the interparticle gap or geometry (i.e. shape) of the structure can drastically change the spectral resonance line shape, which may result in vanishing Fano or Fano-like plasmonic resonance. Notably, the disappearance of Fano resonance has been reported when the interparticle distance between the heterodimers is not close enough (even Fano resonance vanishes for an interparticle distance of 100 nm or even less) [10]. Furthermore, Fano-like plasmonic resonance between two homodimers is very rare because of the absence of quadrupole resonance mode or dark resonance mode. In fact, due to the complex nature of this kind of resonance, no generic set-up has been proposed to achieve robust and stable Fano-like plasmonic resonance in plasmonic nanostructures.

The optical binding force is a relatively new member in the field of optical manipulation. Since the first observation of optical binding force in 1989 [11], it has attracted less attention compared to curl, gradient and scattering forces. In the past, curl, gradient and scattering force based optical manipulation have been given more priority, and have been extensively investigated within the areas of biological science [12, 13], physics [14–17] and chemistry [18]. Perhaps as a result, the optical binding force is neither well defined nor clearly understood and remains unexplored within the framework of the extensive field of optical micromanipulation. In general, the optical binding force can be defined as the interaction among the optically bound particles when they are kept in an intense optical field [11]. It can be a very effective tool to precisely control the mutual attraction and repulsion among optically bound nanoparticles for particle aggregation, crystallization, self-assembly, etc. [19].

In terms of interparticle (surface to surface between nanoparticles) distance, the optical binding force [11, 20–26] can be characterized into two categories: (i) far-field optical binding force [23, 25, 27–31], and (ii) near-field optical binding force [22, 26, 32–40]. The far-field optical binding force can be defined for the objects placed nearly at micrometer (or more than micrometer) distance apart, and the near-field optical binding force can be defined for the objects placed at a distance usually 10 nm to around 250 nm. So far, only a few investigations have been carried out to understand the behavior of near-field and far-field optical binding forces in plasmonic nanostructures. But those investigations have been carried out separately, and also in separate optical configurations for the far field and near field, and they have been mostly restricted to dimers placed in the homogeneous medium [27, 32–34, 40]. As far as we know, no comparative study has been carried out previously in the literature, and no generic optical set-up has been proposed to study the characteristics of both the far-field and near-field optical binding forces in the inhomogeneous medium. Also, as far as we know, no well-established connection between the resonant modes and far-field optical binding force has been reported in the literature until now.

However, few recent investigations have reported the connection between the plasmon resonance and near-field optical binding force [32, 33, 38, 40]. The adjustment of attraction and repulsion between very closely placed nanodimers is known/termed as the reversal of the near-field optical binding force. This novel area is even younger than some of the recent popular areas of optical manipulation, such as the reversal of optical scattering force or passive tractor beams, active tractor beams and optical lateral force. Importantly, controlling the reversal of both the near-field and far-field optical binding forces in the same optical configuration and the impact of the resonant modes in both the near-field and far-field optical binding forces have not been investigated so far. In addition, no generic mechanism has been proposed to achieve a robust and stable Fano-like plasmonic resonance in plasmonic nanostructures, especially in the far-field region.

In this work, we have proposed a generalized mechanism to achieve a controllable, robust and stable Fano-like plasmonic resonance and have shown its remarkable impact in the control of the far-field and near-field optical binding force characteristics. In fact, we have demonstrated a stable Fano-like plasmonic resonance, which is independent of any particular geometrical configuration (i.e. shape of the object) and is even stable for the interparticle distance more than 1 μm for different polarizations of light. The controllable, robust and stable resonance is achieved by the breaking of simple symmetry, considering the distinctly shaped plasmonic (in different geometrical configurations) nanoparticles half immersed in an inhomogeneous dielectric background medium. Also, a comparative study on the far-field and near-field resonant modes along with the characteristics of the reversal of the optical binding force are shown in the same optical set-up (for both Mie and Rayleigh objects). In both the far field and near field, the nanoparticle tetramers are half immersed in the underneath benzene background (a schematic diagram of this configuration is shown in figure 1) under circular polarized illumination.

First, we have started our comparative study with the demonstration of the optical binding force on Rayleigh-range objects, then we have emphasized the Mie-range objects. We have shown that the face to face binding force does not reverse for Rayleigh-sized tetramers, but reverses in both the far and near field for Mie-sized objects. Along with the face to face optical binding force, we have analytically shown another type of binding force for the nanoparticles situated next to each other (we have defined it as the edge to edge binding force). An unusual property of far-field and near-field resonant modes is also observed for our inhomogeneous configuration. We have observed a strong magnetic response in the far-field resonant modes where the near-field resonant modes show a strong electric response. Notably, Lorentz force dynamics have been previously studied to understand the behavior of the near-field optical binding force, but never employed for understanding the behavior of the far-field optical binding force. In our study, we have comparatively studied the Lorentz force dynamics for both the far- and near-field configurations by considering distinctly shaped plasmonic tetramers and have shown some notable differences between them.

Importantly, a clear relationship between resonant modes and the reversal of the far-field optical binding force is shown in our study. Finally, we have shown a way to control the

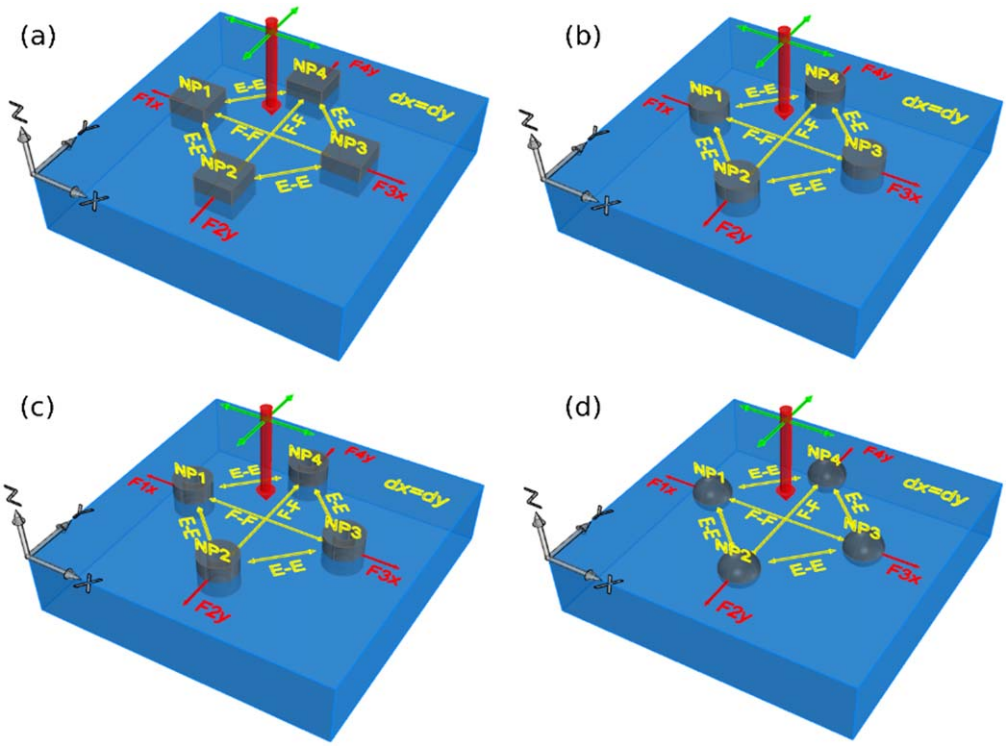

Figure 1. (a)–(d) Schematic diagrams of our generalized tetramer configuration for cube, cylinder, ring and spherical nanoparticles, respectively. Here, distinctly shaped plasmonic nanoparticle tetramers are half immersed in an inhomogeneous dielectric interface. The nanoparticles placed at the '−x', '−y', 'x' and 'y' positions are considered as NP_1, NP_2, NP_3, and NP_4, respectively. F_1, F_2, F_3 and F_4 represent the optical force on NP_1, NP_2, NP_3 and NP_4. F-F represents the face to face binding force between NP_1 and NP_3 and NP_2 and NP_4. Here, d_x and d_y represent the surface to surface distance between the nanoparticles placed at the x-axis and y-axis. In our cases $d_x = d_y$, which indicates that nanoparticles are placed at equal distances from the center. E-E represents the edge to edge optical binding force, which acts through the edge of the nanoparticles.

mutual attraction and repulsion among the nanoparticles based on the refractive index of the lower background medium. Also, we have shown a background refractive-index-dependent tunable optical binding force and controllable resonant modes over the wavelengths.

2. Simulation set-up and methods

In this work, we have used a generalized optical set-up, where the distinctly shaped silver (standard Palik (0–2 μm) [41]) nanoparticles are half immersed in an inhomogeneous dielectric background medium. In the first part of our manuscript, we have shown stable and robust Fano-like plasmon resonance in different geometrical nanostructures (figure 2). In the second part, we have comparatively studied the characteristics of far-field and near-field optical binding forces for a specific tetramer configuration (figure 1). The schematic diagram in figure 1 shows that the four distinctly shaped (cube, cylinder, ring and sphere) plasmonic nanoparticle tetramers are half immersed in the air–benzene interface. We have used both Mie-range objects (mostly) and Rayleigh-range objects for the same generalized optical set-up. But we have mainly focused on Mie-range objects to show the characteristics of the reversal of near-field and far-field optical binding forces. The detailed dimensions (particle size, interparticle distance) of the far field, near field and Rayleigh objects are given in table 1.

Commercial software (Lumerical FDTD) has been used for performing our full-wave simulations [42]. We have illuminated our structure by a circularly polarized wave [43] propagating towards the '$-z$' direction and $E_0 = 1\,\mathrm{V\,m^{-1}}$ (intensity $= 0.001\,176\,\mathrm{W\,m^{-2}}$).

$$\boldsymbol{E} = \boldsymbol{E}_{\mathrm{x}}(z, t) + \boldsymbol{E}_{\mathrm{y}}(z, t). \tag{1}$$

We have used both left- and right-hand circularly polarized light, but no difference in far-field and near-field optical binding force reversal is observed. A significant effect is observed in chiral objects [44–46]. Figure 1 shows that the nanoparticles placed at the '$-x$', '$-y$', 'x' and 'y' axis are considered as NP_1, NP_2, NP_3 and NP_4 respectively. F_1, F_2, F_3 and F_4 represent the optical force on NP_1, NP_2, NP_3 and NP_4. We have calculated both face to face and edge to edge optical binding forces. For calculation of face to face optical binding forces, we have only considered 'x' directional forces (F_x) for the nanoparticles NP_1 and NP_3, as they are placed in the 'x' and '$-x$' position. Similarly, we have considered only 'y' directional forces (F_y) for the particles NP_2 and NP_4, as they are placed in the 'y' and '$-y$' position. Therefore, $\boldsymbol{F}_{\mathrm{bind1}} = \boldsymbol{F}_{1x} - \boldsymbol{F}_{3x}$ represents the face to face binding force between NP_1 and NP_3. Similarly, $\boldsymbol{F}_{\mathrm{bind2}} = \boldsymbol{F}_{2y} - \boldsymbol{F}_{4y}$ indicates the face to face binding force between NP_2 and NP_4. Our configuration is symmetric over the axis, which means that

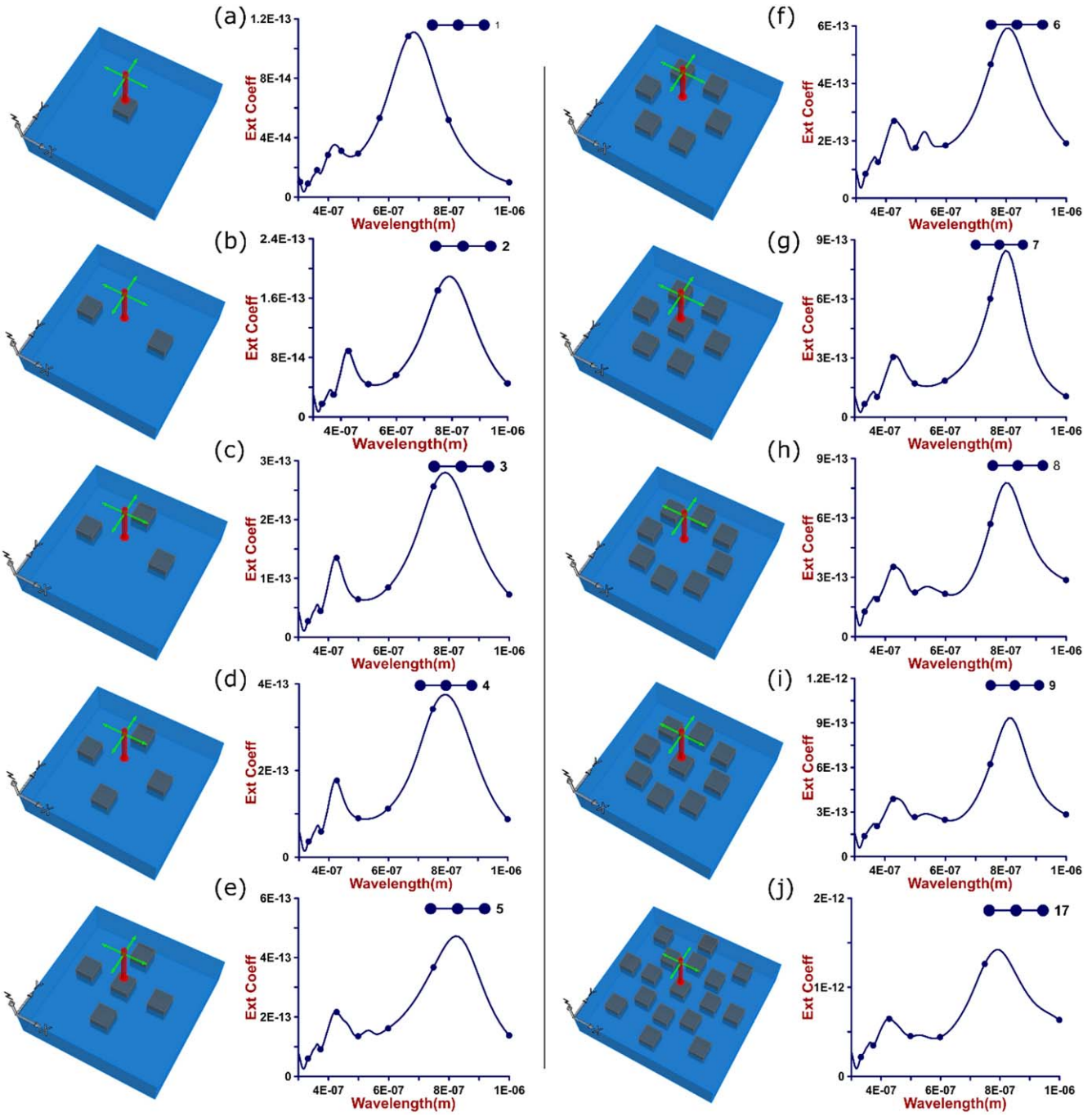

Figure 2. (a)–(j) The extinction spectra curves of cube-shaped plasmonic nanoparticles for different geometrical configurations when the nanoparticles (Mie range) are half suspended in a lower background medium of refractive index 1.87 (which is the highest possible refractive index for liquid medium). The extinction spectra curves show stable Fano-like resonance for all the geometric configurations. It should be noted that the geometrical configurations are not drawn to scale. For example, in figures (b), (d) the surface to surface distances between the plasmonic nanoparticle dimers and tetramers are 1400 nm.

the nanoparticles are placed at an equal distance from the center ($d_x = d_y$). As a result, the optical forces of the individual nanoparticles are $F_{1x} = -F_{3x} = F_{2y} = -F_{4y}$ and $F_{1y} = -F_{3y} = F_{2x} = -F_{4x}$ (details given in supplement 1 available online at stacks.iop.org/CTP/72/045502/mmedia). Hence, the relation between the face to face optical binding force is:

$$\boldsymbol{F}_{\text{bind1}} = \boldsymbol{F}_{1x} - \boldsymbol{F}_{3x} = \boldsymbol{F}_{2y} - \boldsymbol{F}_{4y}[F_{1x} = -F_{3x} = F_{2y} = -F_{4y}] = \boldsymbol{F}_{\text{bind2}}. \quad (2)$$

Therefore, we have used $\boldsymbol{F}_{\text{bind}}$ instead of $\boldsymbol{F}_{\text{bind1}}$ or $\boldsymbol{F}_{\text{bind2}}$ for the face to face optical binding force between the nanoparticles. The positive value of the binding forces represents the attractive binding force, and the negative value represents the repulsive binding force. We have also calculated another type of optical binding force: the edge to edge optical binding force. As the edge to edge optical binding force works through the edge (shown in figure 1), we have considered both 'x' and 'y' components of the forces (F_x and F_y) for

Table 1. The detailed dimensions of the near field, far field and Rayleigh object configuration.

Shape	Dimension of Mie-range objects (nm)	Dimension of Rayleigh-range objects (nm)	Surface to surface distance Rayleigh object set-up (nm)	Surface to surface distance near-field set-up (nm)	Surface to surface distance far-field set-up (nm)
Cube	Length 130 nm	Length 20 nm	40 nm	180 nm	800 nm
Cylinder	Radius 65 nm Height 130 nm	Radius 10 nm Height 20 nm	40 nm	180 nm	800 nm
Ring	Outer radius 65 nm Inner radius 30 nm	Outer radius 10 nm Inner radius 5 nm	40 nm	180 nm	800 nm
Sphere	Radius 65 nm	Radius 10 nm	40 nm	180 nm	800 nm

calculation of the edge to edge binding force of the nanoparticles NP_1, NP_2, NP_3 and NP_4. The details of the edge to edge optical binding force are shown in the results and discussion section.

We have used the time-averaged Minkowski stress tensor [44, 47, 48] and Lorentz force [33, 38, 49, 50] to calculate the total force.

The outside optical force is calculated at $\mathrm{r} = a^{+}$ of the time-averaged Minkowski stress tensor.

$$\langle \boldsymbol{F}^{\mathrm{Out}}_{\mathrm{Total}} \rangle = \sum_{(j)} \oint \langle \overline{\overline{\boldsymbol{T}}}^{\mathrm{out}}_{(j)} \rangle \cdot \mathrm{d}\boldsymbol{s}_{(j)}$$

$$\langle \overline{\overline{\boldsymbol{T}}}^{\mathrm{out}}_{(j)} \rangle = \frac{1}{2}\mathrm{Re}\Big[\boldsymbol{D}_{\mathrm{out}(j)}\boldsymbol{E}^{*}_{\mathrm{out}(j)} + \boldsymbol{B}_{\mathrm{out}(j)}\boldsymbol{H}^{*}_{\mathrm{out}(j)} - \frac{1}{2}\overline{\overline{\boldsymbol{I}}}\,(\boldsymbol{E}^{*}_{\mathrm{out}(j)} \cdot \boldsymbol{D}_{\mathrm{out}(j)} + \boldsymbol{H}^{*}_{\mathrm{out}(j)} \cdot \boldsymbol{B}_{\mathrm{out}(j)})\Big]. \quad (3)$$

Here, $j = 1$ (upper background) and $j = 2$ (lower background) represent the exact background region.

Based on the Lorentz force, the total force (surface force and the bulk force [23, 33, 38, 49, 50]) is:

$$\langle \boldsymbol{F}_{\mathrm{Total}} \rangle = \langle \boldsymbol{F}_{\mathrm{Volume}} \rangle = \sum\nolimits_{(j)} [\langle \boldsymbol{F}_{\mathrm{Bulk}(j)} \rangle + \langle \boldsymbol{F}_{\mathrm{Surf}(j)} \rangle] = \sum_{(j)} \Big[\int \langle \boldsymbol{f}_{\mathrm{Bulk}(j)} \rangle \mathrm{d}v_{(j)} + \int \langle \boldsymbol{f}_{\mathrm{Surface}(j)} \rangle \Big] \mathrm{d}s_{(j)} \quad (4)$$

where

$$\langle \boldsymbol{f}_{\mathrm{Surface}(j)} \rangle = \sigma_e \boldsymbol{E}^{*}_{\mathrm{avg}(j)} + \sigma_m \boldsymbol{H}^{*}_{\mathrm{avg}(j)} = \{\epsilon_o(\boldsymbol{E}_{\mathrm{out}(j)} - \boldsymbol{E}_{\mathrm{in}(j)}) \cdot \hat{\boldsymbol{n}}\} \left(\frac{\boldsymbol{E}_{\mathrm{out}(j)} + \boldsymbol{E}_{\mathrm{in}(j)}}{2} \right)^{*} + \{\mu_0(\boldsymbol{H}_{\mathrm{out}(j)} - \boldsymbol{H}_{\mathrm{in}(j)}) \cdot \hat{\boldsymbol{n}}\} \left(\frac{\boldsymbol{H}_{\mathrm{out}(j)} + \boldsymbol{H}_{\mathrm{in}(j)}}{2} \right)^{*}, \quad (5)$$

$$\langle \boldsymbol{f}_{\mathrm{Bulk}(j)} \rangle = \frac{1}{2}\mathrm{Re}\,[\varepsilon_0(\nabla \cdot \boldsymbol{E}_{\mathrm{in}(j)})\boldsymbol{E}^{*}_{\mathrm{in}(j)} + \mu_0(\nabla \cdot \boldsymbol{H}_{(j)})\boldsymbol{H}^{*}_{\mathrm{in}(j)}] - \frac{1}{2}\mathrm{Re}\,[i\omega(\varepsilon_{s(j)} - \varepsilon_b)\{\boldsymbol{E}_{\mathrm{in}(j)} \times \boldsymbol{B}^{*}_{\mathrm{in}(j)}\} + i\omega(\mu_{s(j)} - \mu_b)\{\boldsymbol{D}^{*}_{\mathrm{in}(j)} \times \boldsymbol{H}_{\mathrm{in}(j)}\}]. \quad (6)$$

The surface force density ($\boldsymbol{f}_{\mathrm{Surface}}$) is calculated just at the boundary, and the bulk force density ($\boldsymbol{f}_{\mathrm{Bulk}}$) is calculated from the interior. Here, ε_s, μ_s are the permittivity and permeability of the nanoparticle itself, and ε_b, μ_b are the background. Here, $\hat{\boldsymbol{n}}$ is an outward pointing normal to the surface, and σ_e and σ_m are the bound electric and magnetic surface charge densities. To the best of our knowledge, the studies of Lorentz force dynamics were only restricted to near field and mostly homogeneous medium [33, 38, 49]. Also, no comparative study was carried out in Lorentz force dynamics for the far field and near field.

The Lorentz force [33, 38, 49, 50] in our equations (2)–(4) is different to the 'external dipolar force' [34, 51–53]. All the numerical calculations are conducted in 3D in full-wave simulations using Lumerical FDTD [54].

The bulk part of the total Lorentz force on a plasmonic object should describe the relative bulk force experienced by the optical molecule:

$$\mathrm{Del}\,F_{\mathrm{Bulk}(1)} = \int [\langle \boldsymbol{f}_{\mathrm{Bulk}(1)} \rangle \mathrm{d}v_{(1)}] - \int [\langle \boldsymbol{f}_{\mathrm{Bulk}(3)} \rangle \mathrm{d}v_{(3)}] \quad (7)$$

$$\mathrm{Del}\,F_{\mathrm{Bulk}(2)} = \int [\langle \boldsymbol{f}_{\mathrm{Bulk}(2)} \rangle \mathrm{d}v_{(2)}] - \int [\langle \boldsymbol{f}_{\mathrm{Bulk}(4)} \rangle \mathrm{d}v_{(4)}]. \quad (8)$$

Here, $\mathrm{Del}\,F_{\mathrm{Bulk}(1)}$ represents the bulk force between NP_1 and NP_3, and $\mathrm{Del}\,F_{\mathrm{Bulk}(2)}$ represents the bulk force between NP_2 and NP_4. At the same time the relative surface force experienced by the optical molecule is:

$$\mathrm{Del}\,\boldsymbol{F}_{\mathrm{Surf}(1)} = \int [\langle \boldsymbol{f}_{\mathrm{Surf}(1)} \rangle \mathrm{d}v_{(1)}] - \int [\langle \boldsymbol{f}_{\mathrm{Surf}(3)} \rangle \mathrm{d}v_{(3)}] \quad (9)$$

$$\mathrm{Del}\,\boldsymbol{F}_{\mathrm{Surf}(2)} = \int [\langle \boldsymbol{f}_{\mathrm{Surf}(2)} \rangle \mathrm{d}v_{(2)}] - \int [\langle \boldsymbol{f}_{\mathrm{Surf}(4)} \rangle \mathrm{d}v_{(4)}]. \quad (10)$$

Here, $\mathrm{Del}\,\boldsymbol{F}_{\mathrm{Surf}(1)}$ represents the surface force between NP_1 and NP_3, and $\mathrm{Del}\,\boldsymbol{F}_{\mathrm{Surf}(2)}$ represents the surface force between NP_2 and NP_4.

It should be noted that:

$$\boldsymbol{F}_{\mathrm{Bind1}} = \mathrm{Del}\,\boldsymbol{F}_{\mathrm{Bulk1}} + \mathrm{Del}\,\boldsymbol{F}_{\mathrm{Surf1}}. \quad (11)$$

$$\boldsymbol{F}_{\mathrm{Bind2}} = \mathrm{Del}\,\boldsymbol{F}_{\mathrm{Bulk2}} + \mathrm{Del}\,\boldsymbol{F}_{\mathrm{Surf2}}. \quad (12)$$

In our cases $\mathrm{Del}\,\boldsymbol{F}_{\mathrm{Surf}(1)} = \mathrm{Del}\,\boldsymbol{F}_{\mathrm{Surf}(2)}$, and $\mathrm{Del}\,\boldsymbol{F}_{\mathrm{Bulk}(1)} = \mathrm{Del}\,\boldsymbol{F}_{\mathrm{Bulk}(2)}$. So, we have used $\mathrm{Del}\,\boldsymbol{F}_{\mathrm{Surf}}$ and $\mathrm{Del}\,\boldsymbol{F}_{\mathrm{Bulk}}$ to represent the surface force and bulk force, respectively. We have already mentioned that throughout the paper we have shown $\boldsymbol{F}_{\mathrm{bind}}$ instead of using both $\boldsymbol{F}_{\mathrm{bind1}}$ and $\boldsymbol{F}_{\mathrm{bind2}}$.

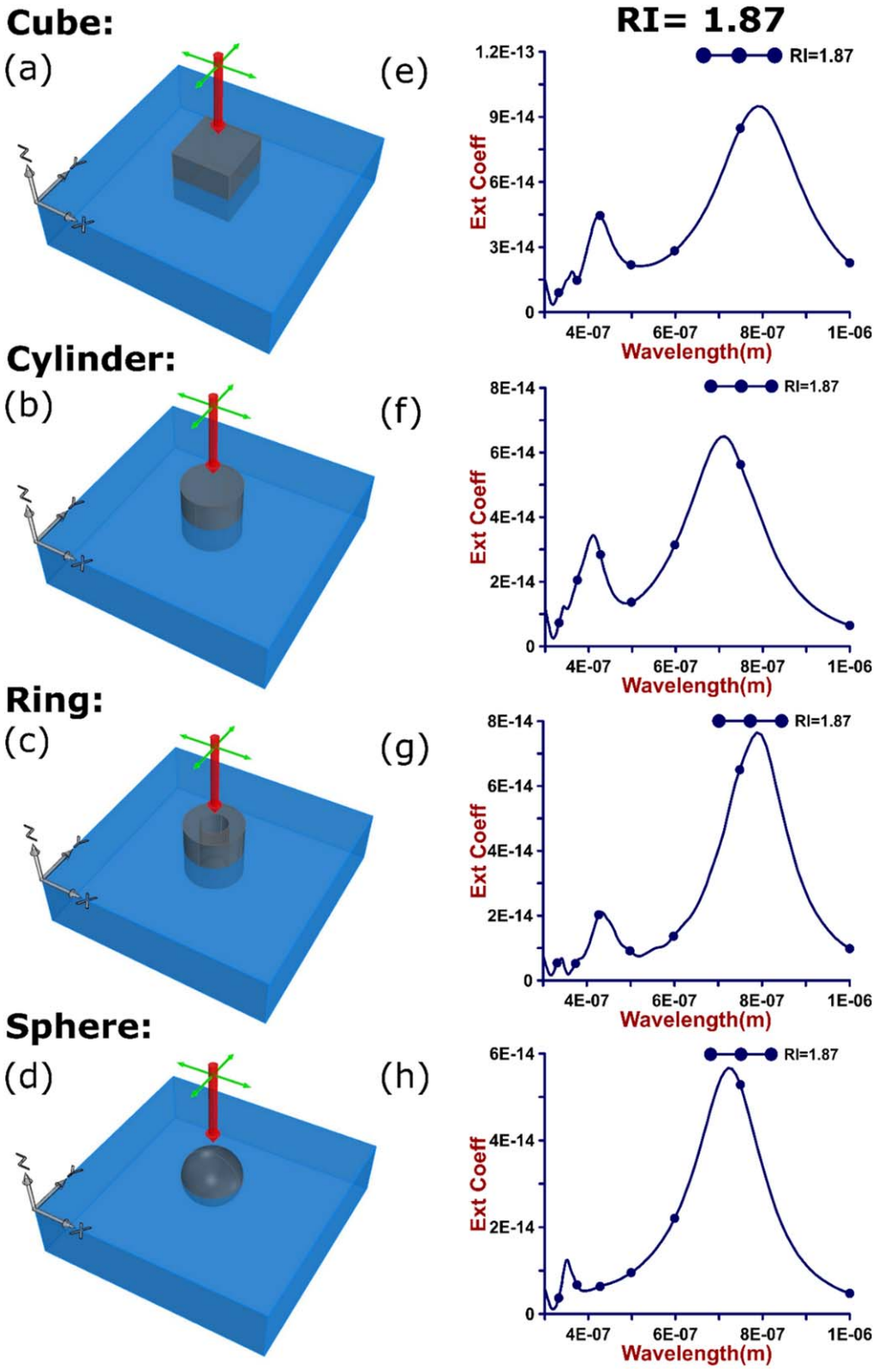

Figure 3. (a)–(d) Schematic diagrams of distinctly shaped single plasmonic nanoparticles half immersed in inhomogeneous dielectric background medium. Figures (e)–(h) show the extinction spectra curves of cube-, cylinder-, sphere and ring-shaped nanoparticles for 1.87 refractive index underneath background medium, which show stable Fano-like resonance.

3. Results and discussion

We have commenced our study by showing robust and stable Fano-like plasmonic resonance of distinctly shaped (cube, cylinder, ring and sphere) Mie-range plasmonic nanoparticles for our proposed optical set-up (figure 1). Figures 2(a)–(j) show a stable Fano-like resonance for cube-shaped plasmonic nanoparticles in different geometrical arrangements (i.e. from

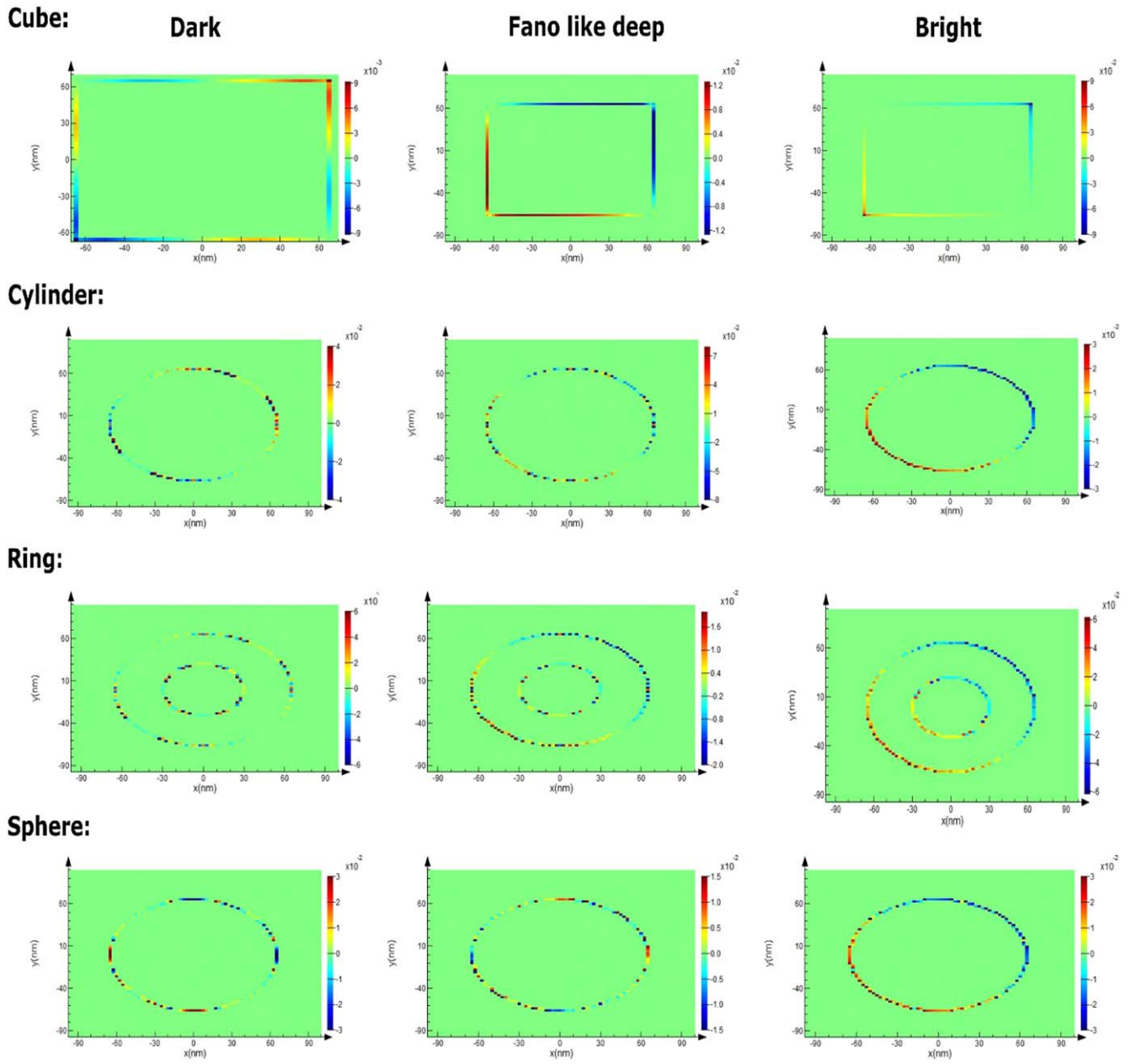

Figure 4. The charge distributions at dark, Fano-like deep and bright resonant modes for distinctly shaped single plasmonic nanoparticles half immersed in a high refractive index (1.87) liquid underneath background medium. The optical set-up is shown in figures 2(a)–(d). The electric field distribution is obtained directly from the simulation results found in the commercial software Lumerical FDTD [42].

a single plasmonic nanoparticle to a cluster of 17 nanoparticles). The nanoparticles are half immersed in an underneath dielectric background medium, and the refractive index of the background medium is 1.87, which is the highest possible refractive index for liquid materials [58]. Achieving this kind of stable and robust Fano-like resonance for distinctly shaped plasmonic nanoparticles in different geometrical configurations is quite remarkable. This is because Fano resonance was reported to have vanished when the interparticle gap or particle size was not precisely controlled, and even specific geometric configurations were required to achieve such stable Fano-like resonance. For example, finite plasmonic nanoclusters (i.e. tetramer, pentamer, hexamer, heptamer, etc.) show sharp Fano-like plasmonic resonance when they are placed very close to each other in a specific geometrical configuration [5–7]. Those Fano-like resonances vanish when the interparticle distance is greater than a few nanometers and can sometimes disappear due to the exclusion of the central particle. We have overcome those difficulties and shown a stable Fano-like resonance for cube-shaped nanoparticles, where the central particle is not present even when the interparticle distance between the nanoparticles is very large (1400 nm figure 2(d)).

A stable Fano-like plasmon resonance can also be found in cylindrical, ring and spherical plasmonic nanoparticles for similar geometrical arrangements, which are shown in

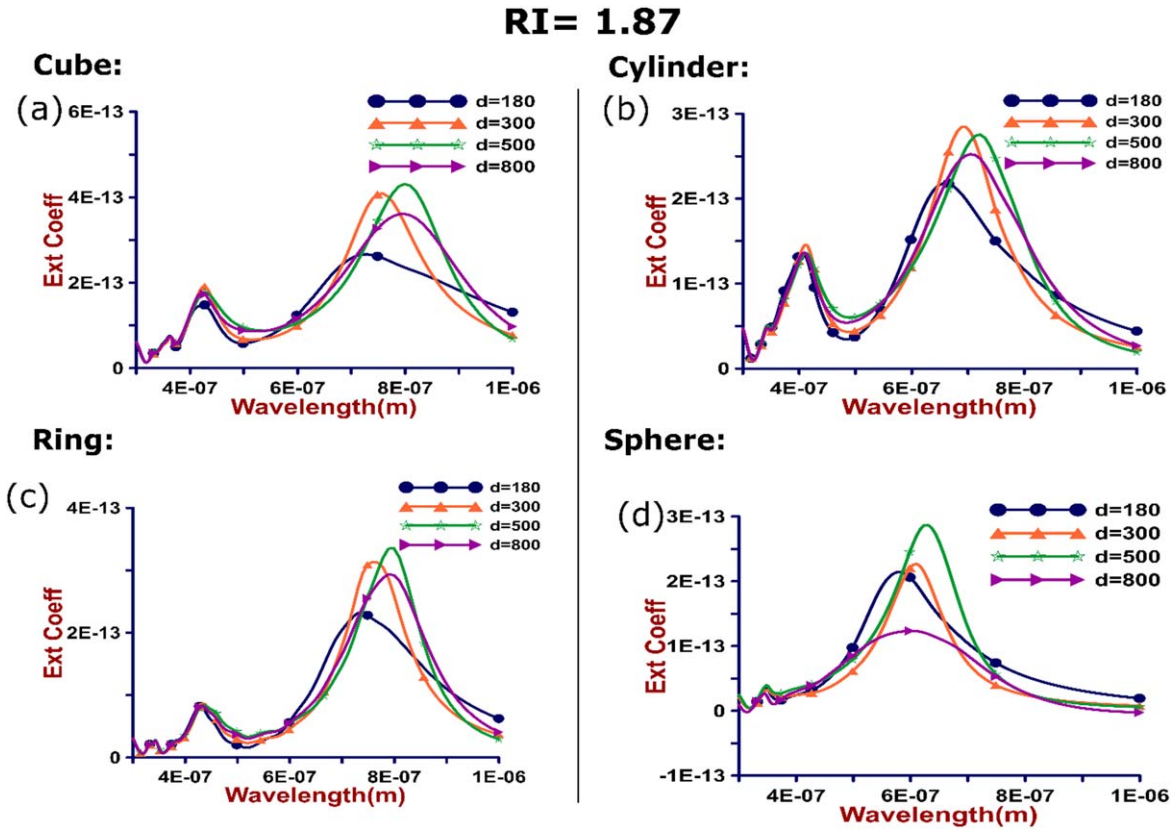

Figure 5. The extinction spectra curve when the Mie-range distinctly shaped nanoparticle tetramers are half immersed in an inhomogeneous dielectric background for different interparticle distances ($d = d_x = d_y =$ 800, 500, 300, 180 nm). (a)–(d) The extinction spectra curves of cube-, cylinder-, sphere and ring-shaped nanoparticle tetramers, respectively, for the underneath background medium of refractive index = 1.87.

(supplement S2) which shows the robustness of our proposed set-up. Along with circular polarized light, we have also observed stable Fano-like resonance for single polarized (x and y polarized) light for our proposed configuration, which is not shown in our article.

To properly understand the origin of such stable Fano-like resonance, we can consider two factors:

(i) interaction of the plasmonic nanoparticles with the underneath background medium, and
(ii) interaction of the plasmonic nanoparticles with each other (for multiple particles).

We have considered a single plasmonic nanostructure (figure 3) half immersed in the underneath dielectric background medium to clearly understand the interaction between the plasmonic nanoparticles with the underneath background medium. The extinction spectra curves of figures 3(e)–(h) show stable Fano-like resonance, but this kind of resonance is not found if individual plasmonic nanostructures are placed in air or homogeneous medium, or placed above the dielectric substrate [10, 23]. In our case, the appearance of underneath background medium fulfils the fundamental criterion of Fano resonance. The fundamental criterion of Fano and Fano-like plasmonic resonance is the constructive and destructive interference between the broad resonant mode and narrow resonant mode. The resonant mode at higher wavelengths is termed the bright resonant mode, and the resonant mode at lower wavelengths is termed the dark resonant mode. The charge distribution of figure 4 in the bright resonant mode shows a purely dipolar behavior. But in the dark resonant mode, it shows a higher-order resonance (mode not purely quadrupolar). At the Fano-like deep position, the charge distribution is a mixture of bright and dark resonant modes. This interaction between the bright dipolar resonant mode and the higher-order dark resonant mode leads to stable higher-order Fano-like resonance, which is quite different to that presented in [55]. In our case, the image charge-induced surface plasmon mode leads to the hybridization of intra-nanoparticle plasmonic modes [42, 56, 57], which further leads to stable higher-order Fano-like plasmonic resonance in our proposed optical system. A high refractive index (RI = 1.87) background medium shows a comparatively strong Fano-like resonance due to the dielectric screening factor $(\varepsilon_s - 1)/(\varepsilon_s + 1)$. The higher dielectric screening leads to stronger hybridization of intra-nanoparticle plasmonic modes. As a result, more stable Fano-like resonance is found. This phenomenon leads to another notable conclusion: the underneath background medium can be used as a controlling parameter to increase or decrease the strength of Fano-like resonance.

Apart from background-mediated interaction, the interaction among the nanoparticles also has an impact on stable and robust Fano-like resonance. We have chosen a tetramer configuration (figure 1) to show the interaction among the

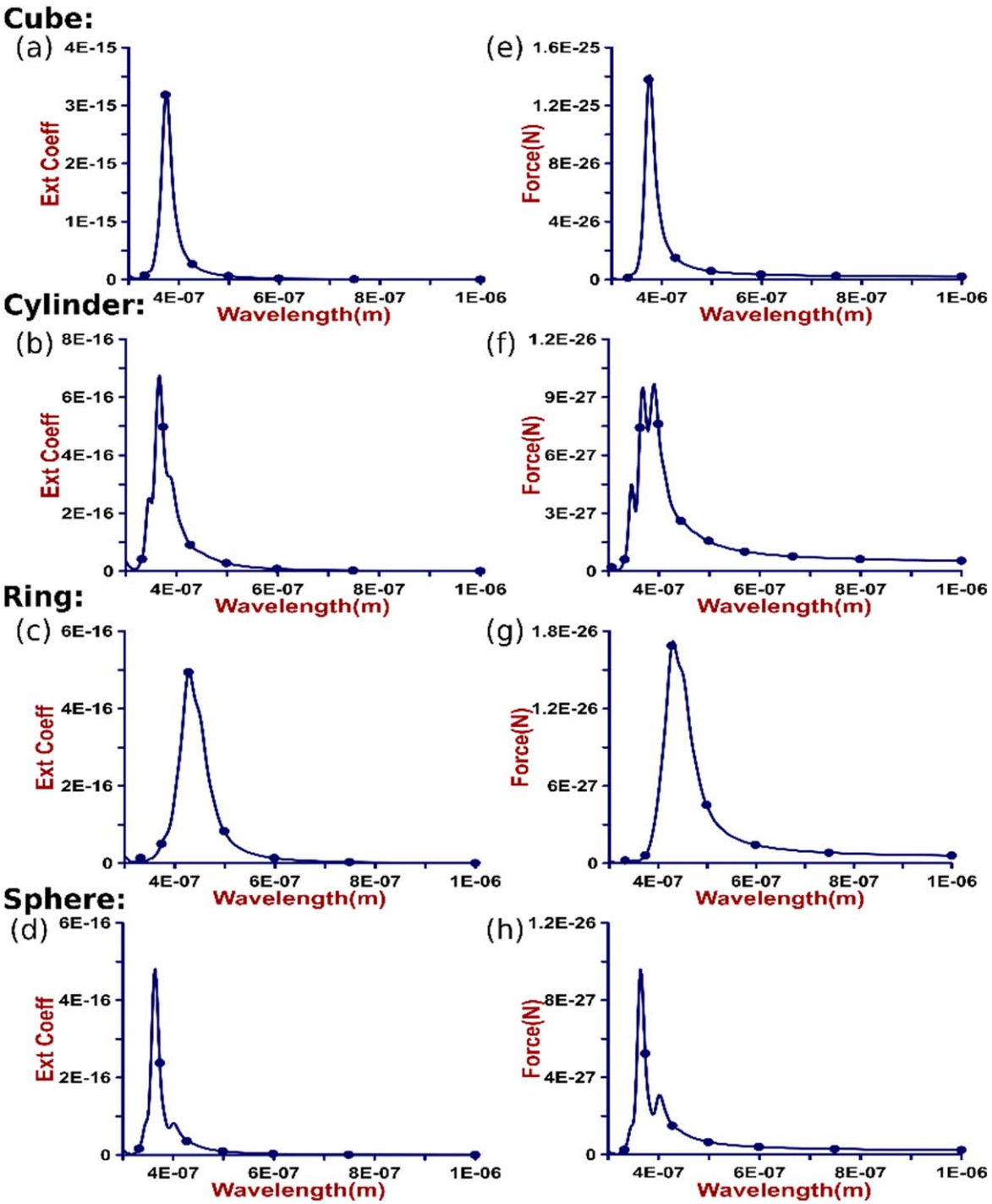

Figure 6. (a)–(d) Extinction spectra curves of distinctly shaped Rayleigh-range plasmonic tetramers placed in an inhomogeneous background (refractive index = 1.50). Figures (e)–(h) represent the binding force curves of cube-, cylinder-, ring- and spherical-shaped tetramers, respectively. The binding force does not reverse for Rayleigh-range objects.

nanoparticles. Figure 5 shows the extinction spectra curves of distinctly shaped plasmonic nanoparticle tetramers at different interparticle distances ($d = d_x = d_y = 800$ nm, 500 nm, 300 nm, 180 nm). With the decrease in the interparticle distance, the interaction among the distinctly shaped plasmonic nanoparticle tetramers increases due to their interference field. As a result, figure 5 shows a comparatively stronger Fano-like resonance; when the interparticle distance is very small (180 nm) compared to the interparticle distance 800 nm. But figure 5 also reveals that the effect of the interparticle gap distance is negligible compared to the effect of the underneath background medium.

It is important to note that our proposed optical set-up does not show Fano-like plasmonic resonance for Rayleigh-range objects, but it shows stable and robust Fano-like resonance only for Mie objects. Rayleigh-range nanoparticle tetramers (figures 6(a)–(d)) do not show any higher-order resonant mode, but only show a broad dipolar resonant mode.

It is due to the internal excitation of multipoles (i.e. quadrupoles, hexapoles, etc) occurring in Mie objects (more details in the supplementary article of [58]); this behavior is not common in Rayleigh-range objects. As a result, hybridization of the bright and dark resonant modes does not occur in Rayleigh objects and, therefore, the fundamental criterion of Fano-like plasmonic resonance is not fulfilled in Rayleigh objects. It is worth mentioning that the mechanism of Fano-like resonance in dielectric nanostructures [23, 59–61] is completely different to plasmonic nanostructures, as dielectric nanostructures have no distinct plasmon modes.

Based on the discussion above, it can be said that in our proposed optical set-up, robust and stable Fano-like plasmonic resonance for Mie objects mainly originates from the interaction of the plasmonic nanoparticles with the underneath background medium, and almost provides an interparticle distance independent and geometry independent Fano-like resonance. Although our resonant mode fulfils all the criterion of Fano resonance, throughout the paper we have described it as Fano-like plasmonic or Fano-like resonance due to its unusual line shape.

4. Optical force behavior of Mie and Rayleigh-range plasmonic nanoparticle tetramers

In this section, we have chosen a specific plasmonic tetramer configuration (cf figure 1) to show the characteristics of the far-field and near-field optical binding forces, and the impact of the resonant modes on both the far-field and near-field optical binding forces.

Figure 6 shows the optical binding force for Rayleigh-sized metallic nanoparticle tetramers does not reverse, when they are half immersed in an inhomogeneous dielectric background or they are kept in a homogeneous medium (supplement S3). Figures 6(e)–(h) show that the face to face optical binding forces between the small metallic nanoparticle tetramers are always attractive, and the maximum value of the face to face optical binding force is observed exactly at that resonant peak for our taken wavelength region (300 nm to 1000 nm). Although the optical binding force among Rayleigh objects is always attractive in our configuration, we can observe both positive and negative values of the electric dipole moment (supplement S4). Still, no reversal of the face to face optical binding force is observed for Rayleigh-range objects. We have defined the real part of the electric dipole moment of an object as [62]:

$$p = \mathrm{Re}\left[\int \mathrm{i}\omega[(\in_s - \in_0)E_{\mathrm{in}}]\mathrm{d}v\right]. \tag{13}$$

The real part of the electric dipole moment (for NP_1 and NP_3, and NP_2 and NP_4) reverses at exactly the same wavelength. It means that the relative dipole moment always remains the same between the face to face particles. Therefore, the optical binding force between the Rayleigh-range metallic nanoparticle tetramers is always attractive to our optical configuration. Our study completely matches with the previous study carried out on plasmonic spherical dimers in [34], which has been explained based on the relative electric polarizability of the face to face nanoparticle. It means that the optical binding force does not reverse for distinctly shaped Rayleigh-range plasmonic nanoparticle tetramers.

But in this part, we have shown the binding force reverses for the Mie-range plasmonic nanoparticle tetramers. Based on the surface to surface interparticle distance for the same optical set-up, we have classified our tetramer configuration into two parts:

(i) far field (interparticle distance = 800 nm), and
(ii) near field (interparticle distance = 180 nm).

Although, the optical binding force reverses for both cases of far field and near field, there are still some interesting differences and similarities between the binding force reversal of the far-field and near-field configurations. The extinction spectra curves for the far-field configuration in figures 7(i)–(l) show strong resonant peaks at higher wavelengths but relatively weak resonant peaks at lower wavelengths. But for the near-field configuration, the extinction spectra curves of figures 7(a)–(d) show two distinct and more prominent resonant peaks at lower and higher wavelengths. Table 2 shows the wavelengths at which bright, dark and Fano-like resonance occurs for near-field and far-field configurations. The interaction between the underneath dielectric background and plasmonic nanoparticles is almost the same for both the near field and far field, but due to the interference field the interactions among the nanoparticles change with the change in the interparticle distance among plasmonic tetramers. As a result, a more visible bright and dark resonant peak is observed in the near-field configuration compared to the far field. For the same reason, a comparatively stronger and more stable Fano-like resonance is observed in the near-field configuration, which mainly originates due to the background-mediated destructive interference of the bright and dark resonant modes (a detailed discussion is given in the previous section).

If we analyze the resonant behavior of the far-field and near-field resonant modes, we find some interesting differences.

The vector diagrams of electric field distribution in figure 8 show some remarkable properties. In the far-field configuration, the electric field distributions in figure 8 show circulating field behavior for distinctly shaped tetramers. Although the circulating field behavior in the far field is not present in the Fano-like deep region, the circulating electric field is clearly visible in bright and dark resonant modes. On the other hand, the electric field distributions in the near-field configuration show no circulating electric field behavior. The circulating electric field distribution in the far-field set-up indicates the dominant magnetic nature of the resonant modes. On the other hand, non-circulating field behavior in near-field configurations indicates the electric nature of the resonant modes. This kind of circulating electric field behavior of the far field is quite unusual and not commonly observed in such types of simple geometric configurations [63–68]. Our observation of the magnetic nature of the resonant modes in such a simple geometry may give an important insight towards the negative refractive-index-based metamaterials.

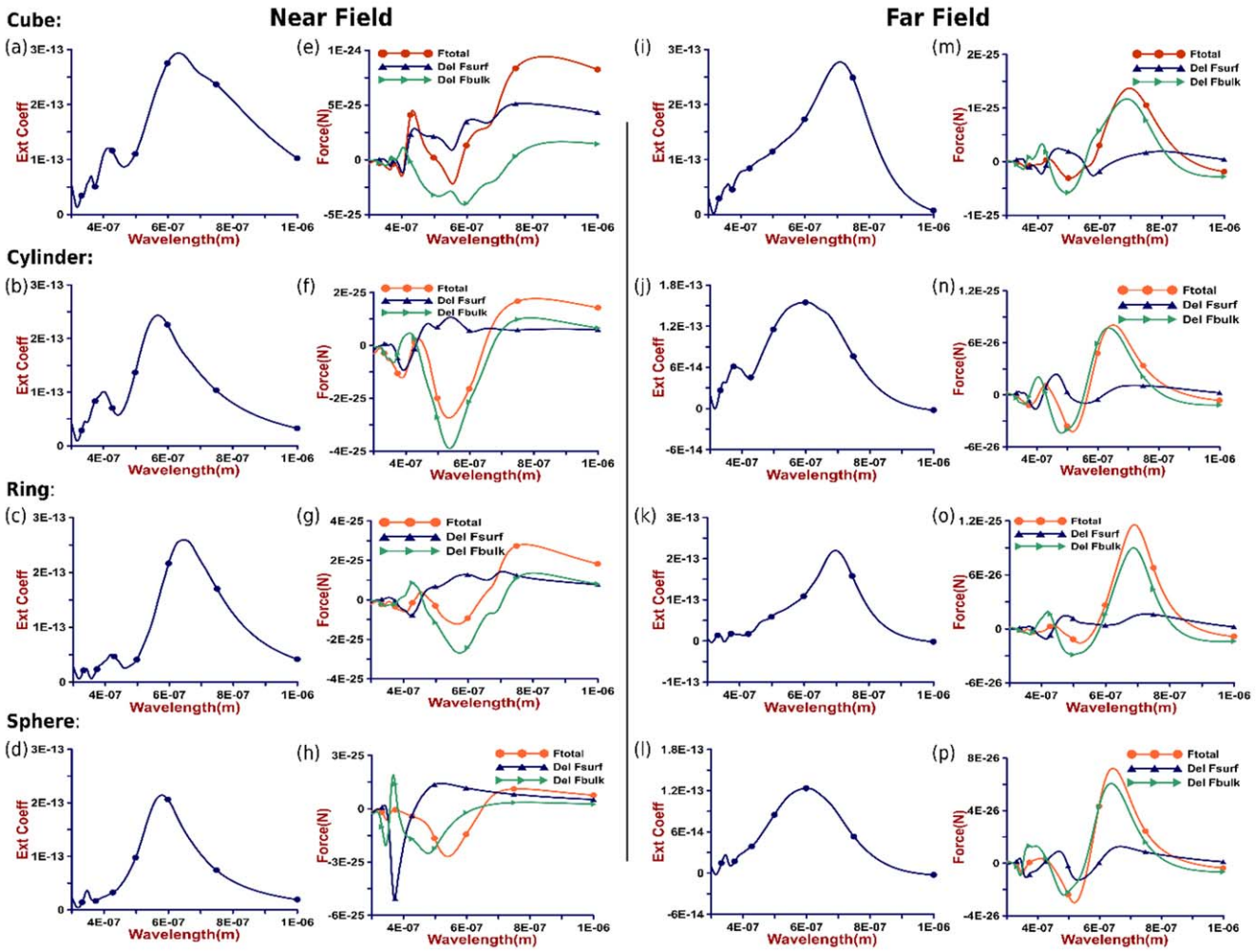

Figure 7. The first two columns represent the near-field ((a)–(d)) extinction spectra and ((e)–(h)) binding force, and the next two columns represent the far-field ((i)–(l)) extinction spectra and ((m)–(p)) binding force for cube, cylinder, ring and spherical nanoparticle tetramers, respectively. Mie-range plasmonic tetramers are placed in a background medium of 1.50 refractive index. In our geometry, nanoparticles are placed at equal distances from the center. Thus, for our configuration $\boldsymbol{F}_{\text{bind}} = \boldsymbol{F}_{\text{bind1}} = \boldsymbol{F}_{\text{bind2}}$. As a result, F_{bind} represents the binding force between NP_1 and NP_3, and NP_2 and NP_4. The positive value and the negative values of the binding forces, respectively, represent the attractive binding force and the repulsive binding force. Lorentz force components of the binding force are represented by the (Del F_{Surf}) surface force and (Del F_{Bulk}) bulk force.

Table 2. The wavelength at which bright, dark and Fano-like resonance occurs for near-field and far-field configurations.

Shape	Near field bright (nm)	Near field deep (nm)	Near field dark (nm)	Far field bright (nm)	Far field deep (nm)	Far field dark (nm)
Cube	637	464	418	713	371	360
Cylinder	570	446	401	604	421	376
Ring	651	460	421	696	412	378
Sphere	581	371	347	604	360	345

5. Lorentz force dynamics of far- and near-field face to face optical binding forces and its relationship with the resonant modes

As far as we know, Lorentz force dynamics for far-field configurations has not yet been discussed in any previous literature. In this section, we have comparatively described the face to face Lorentz force dynamics for both near and far-field tetramers, and we have also shown their relationship with the resonant modes. In addition, we have shown the impact of the resonant modes in both far-field and near-field optical binding forces.

The Lorentz force characteristics for near-field and far-field optical binding forces seem similar, but there are several significant differences between them. The binding force curves of figure 7 show that in near dark resonant mode the

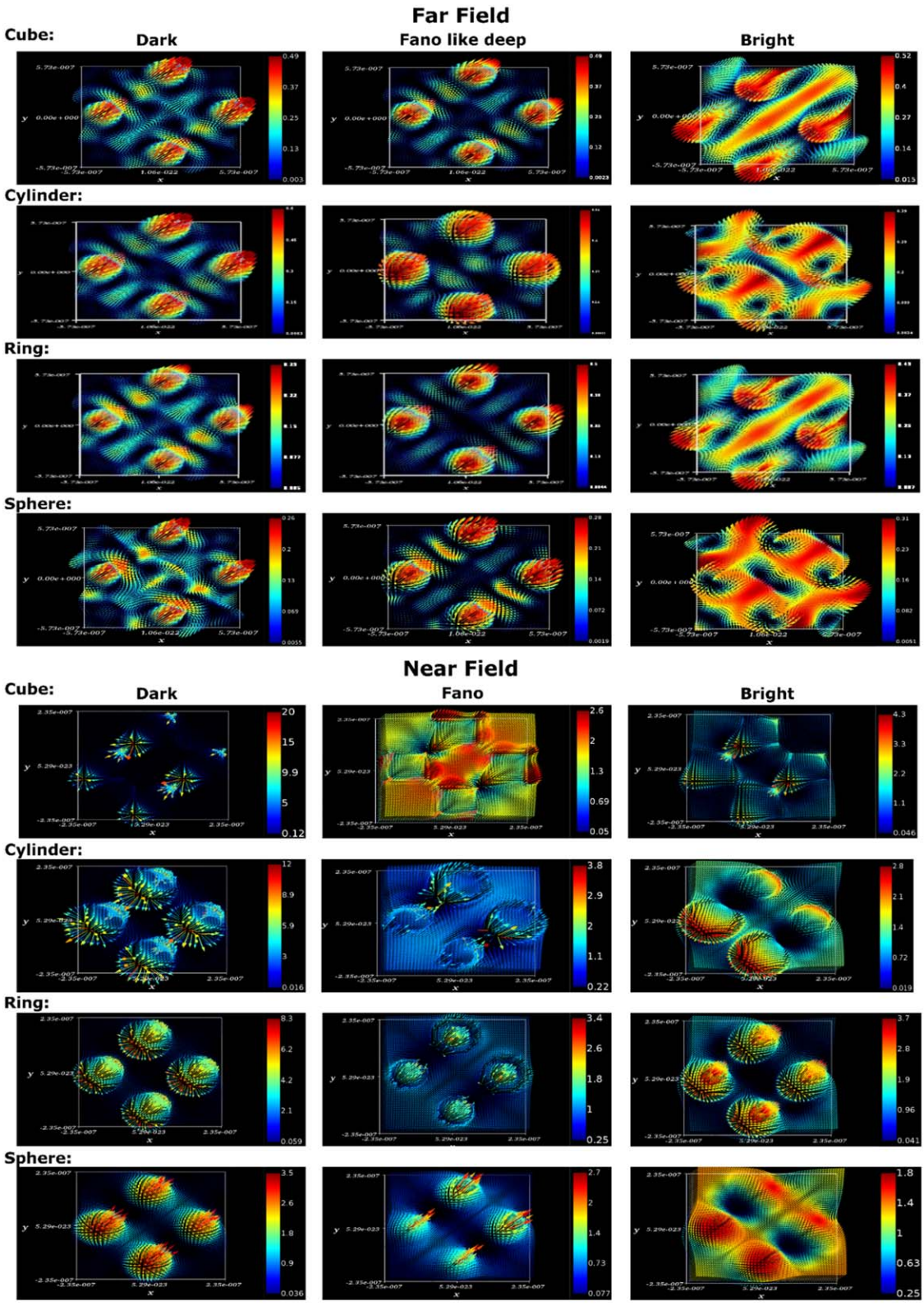

Figure 8. The top view of electric field distribution for cube-, cylinder-, ring- and sphere-shaped nanoparticle tetramers at dark, Fano-like deep and bright resonant modes for far-field and near-field configurations. The first, second and third rows, respectively, show the dark, Fano-like deep and bright resonant modes for cube-, cylinder-, ring- and sphere-shaped nanoparticle tetramers. Table 2 shows the wavelength at which bright, dark and Fano-like deep resonance occur for near-field and far-field configurations. The far-field electric field distribution shows circulating field behavior, but the electric field distribution shows no circulating behavior. The vector diagram of the electric field distribution is obtained directly from the simulation results found in the commercial software Lumerical FDTD [42].

optical binding force reverses (except for the near-field spherical tetramer figure 7(h)) for both the near field and far field. In particular, the near-field configuration (figures 7(e)–(h)) shows that the face to face optical binding force becomes negative to positive and reaches its local maximum positive value where the effect of the bulk force (Del F_{Bulk}) is negligible. It means that the total binding force near the dark resonant mode is mainly dominated by the surface force (Del F_{Surf}) for the near-field configuration. But a completely different scenario is observed in the far field face to face optical binding force in figures 7(m)–(p). Near the reversal point, the far-field optical binding force curves (figures 7(m)–(p)) show a gradual increase in the surface force (Del F_{Surf}) and a maximum value of the bulk force (Del F_{Bulk}). It specifies that the combination of both the surface force (Del F_{Surf}) and bulk force (Del F_{Bulk}) is responsible for the binding force reversal (− to +) of the total force for the far-field configuration.

In both the near-field and far-field set-up, the next binding force reversal is found just after the Fano-like deep position. Also, the binding force reaches its maximum repulsive value between the Fano deep and next reversal point. The binding force curves of figures 7(e)–(h) and (m)–(p) show that the reversal (positive to negative) and minimum binding force near the Fano-like deep position originate mainly due to the dominance of the repulsive bulk force (Del F_{Bulk}), where the surface force (Del F_{Surf}) effect is negligible compared to the bulk force (Del F_{Bulk}) in both the far field and near field. But if we take a closer look, we might see that the surface force (Del F_{Surf}) is more effective in the near-field configuration compared to the far field.

Finally, the next reversal occurs just before the bright resonant mode. The binding force reversal reaches its maximum positive value for both the far-field and near-field configurations. In the far-field configuration, the binding force reversal and maximum binding force are observed mainly due to the dominance of the bulk force (Del F_{Bulk}), where the surface force (Del F_{Surf}) is negligible. But in the near-field set-up, the surface force (Del F_{Surf}) shows a significant effect compared to the far field. Hence, the near bright resonant mode optical binding force has the combined effect of both the surface force and bulk force.

Subsequently, the discussion above demonstrates that the far-field optical binding force is mainly dominated by the bulk force (Del F_{Bulk}), where near-field optical binding force is dominated by both the surface (Del F_{Surf}) force and bulk force (Del F_{Bulk}). A clear insight regarding this observation can be found by considering the face to face distance among nanoparticles in the far-field and near-field set-ups. The surface to surface distance of distinctly shaped nanoparticle tetramers in the near-field configuration is 180 nm, where the surface to surface distance in the far-field configuration is 800 nm. As a result, in the near-field optical binding force we find a more effective surface force (Del F_{Surf}) compared to the far field.

If we take a look at the binding force curve in figure 7(e) (binding force curve for the cube), it will make our claim regarding the dominance of the surface force (Del F_{Surf}) clearer. The cube has greater effective face to face surface area compared to the cylindrical-, ring- and spherical-shaped nanoparticles. Therefore, in the near-field configuration the cube-shaped tetramer shows more effective surface force compared to the other three shapes. Notably, figure 7 also shows that the magnitude of the far-field optical binding force is much lower compared to the near-field optical binding force.

6. Edge to edge optical binding force among the nanoparticles placed close to each other

In this section, we have analytically shown the calculation of the edge to edge optical binding force among the nanoparticles in both the near field and far field. When we have calculated face to face optical binding forces, we have only considered 'x' directional forces (F_x) for the particles (NP_1 andNP_3) placed in the 'x' and '-x' positions. Similarly, we have considered 'y' directional forces (F_y) for the particles (NP_2 and NP_4) placed in the 'y' and '-y' positions. But to calculate the edge to edge binding force we have to consider both F_x and F_y for the nanoparticles NP_1, NP_2, NP_3 and NP_4. We have already shown $F_{1x} = -F_{3x} = F_{2y} = -F_{4y}$ and $F_{1y} = -F_{3y} = F_{2x} = -F_{4x}$ for both the near-field and far-field regions (supplement S1). As the edge to edge optical binding force acts through the edge of the nearest nanoparticle, the edge to edge optical binding force between the nanoparticles can be written as

The edge to edge optical binding force between NP_1 and NP_2:

$$\begin{aligned}\boldsymbol{F}_{EE-12} &= \boldsymbol{F}_2 - \boldsymbol{F}_1 = \boldsymbol{F}_{2x} + \boldsymbol{F}_{2y} - \boldsymbol{F}_{1x} - \boldsymbol{F}_{1y} \\ &= \boldsymbol{F}_{2x} + \boldsymbol{F}_{2y} - \boldsymbol{F}_{2y} - \boldsymbol{F}_{2x} \\ &[\boldsymbol{F}_{1x} = \boldsymbol{F}_{2y},\ \boldsymbol{F}_{1y} = \boldsymbol{F}_{2x}] = 0.\end{aligned}$$

The edge to edge optical binding force between NP_2 and NP_3:

$$\begin{aligned}\boldsymbol{F}_{EE-23} &= \boldsymbol{F}_3 - \boldsymbol{F}_2 = \boldsymbol{F}_{3x} + \boldsymbol{F}_{3y} - \boldsymbol{F}_{2x} - \boldsymbol{F}_{2y} \\ &= \boldsymbol{F}_{3x} + \boldsymbol{F}_{3y} - (-\boldsymbol{F}_{3y}) - (-\boldsymbol{F}_{3x}) \\ &[\boldsymbol{F}_{2x} = -\boldsymbol{F}_{3y},\ \boldsymbol{F}_{2y} = -\boldsymbol{F}_{3x}] \\ &= 2(\boldsymbol{F}_{3x} + \boldsymbol{F}_{3y}) = -2(\boldsymbol{F}_{2x} + \boldsymbol{F}_{2y}).\end{aligned}$$

The edge to edge optical binding force between NP_3 and NP_4:

$$\begin{aligned}\boldsymbol{F}_{EE-34} &= \boldsymbol{F}_4 - \boldsymbol{F}_3 = \boldsymbol{F}_{4x} + \boldsymbol{F}_{4y} - \boldsymbol{F}_{3x} - \boldsymbol{F}_{3y} \\ &= \boldsymbol{F}_{4x} + \boldsymbol{F}_{4y} - \boldsymbol{F}_{4y} - \boldsymbol{F}_{4x}[\boldsymbol{F}_{3x} = \boldsymbol{F}_{4y}, \boldsymbol{F}_{3y} = \boldsymbol{F}_{4x}] = 0.\end{aligned}$$

The edge to edge optical binding force between NP_4 and NP_1:

$$\begin{aligned}\boldsymbol{F}_{EE-41} &= \boldsymbol{F}_1 - \boldsymbol{F}_4 = \boldsymbol{F}_{1x} + \boldsymbol{F}_{1y} - \boldsymbol{F}_{4x} - \boldsymbol{F}_{4y} \\ &= \boldsymbol{F}_{1x} + \boldsymbol{F}_{1y} - (-\boldsymbol{F}_{1y}) - (-\boldsymbol{F}_{1x}) \\ &[\boldsymbol{F}_{1x} = -\boldsymbol{F}_{4y},\ \boldsymbol{F}_{1y} = -\boldsymbol{F}_{4x}] \\ &= 2(\boldsymbol{F}_{1x} + \boldsymbol{F}_{1y}) = -2(\boldsymbol{F}_{4x} + \boldsymbol{F}_{4y}).\end{aligned}$$

The theoretical calculation above is supported by the top view of the electric field distribution of the near-field and

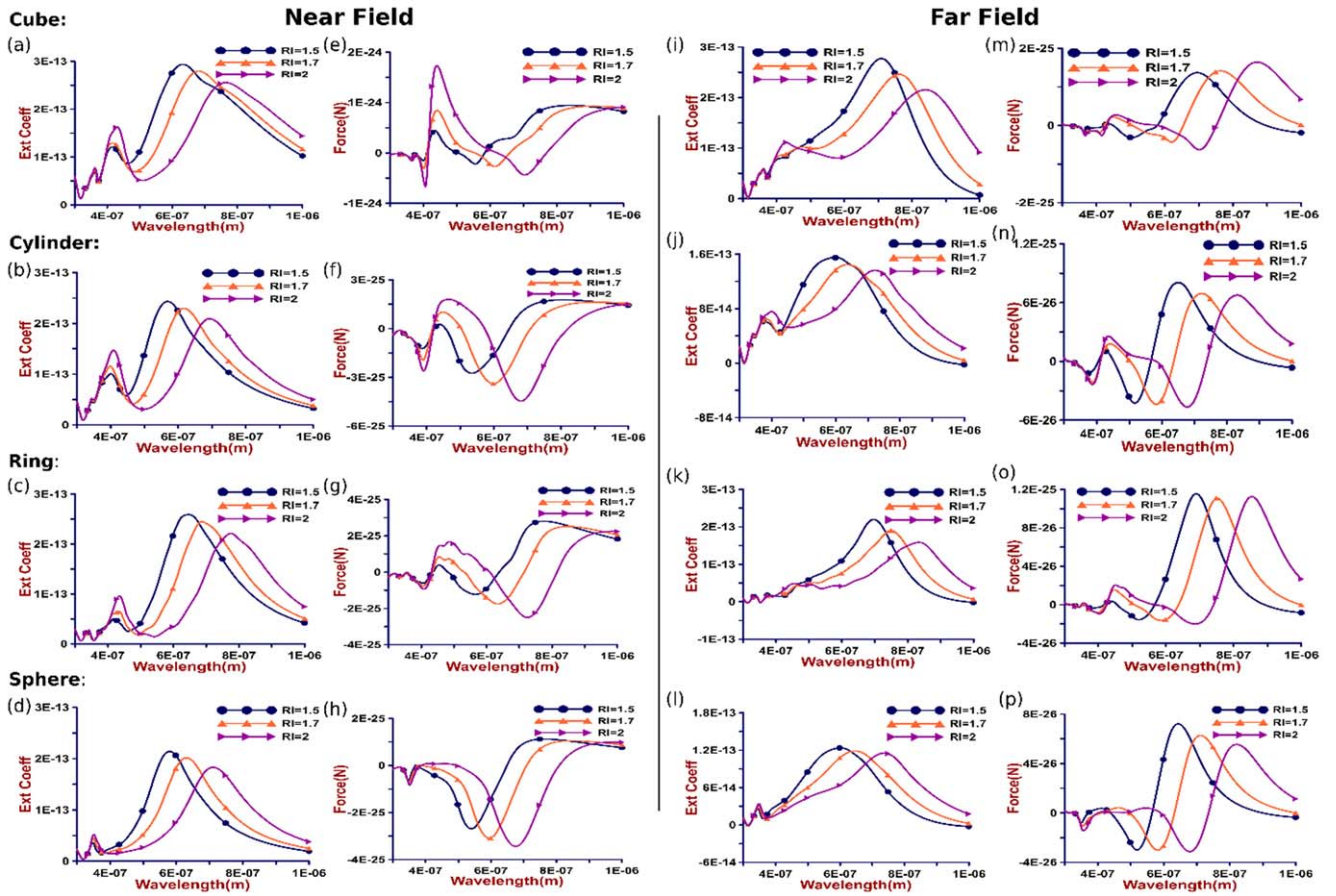

Figure 9. The extinction spectra and binding force curves of both the near field and far field for three different refractive index values (RI = 1.5, 1.7, 2 respectively) of the three distinct lower background media, respectively. The first and second columns represent the near field, and the third and fourth columns represent the corresponding force curves. Figures (a)–(e) represent the extinction spectra, and figures (f)–(h) represent the binding force curves for the near-field tetramers. Similarly, figures (i)–(l) represent the extinction spectra, and figures (m)–(p) represent the binding force curves for the near-field tetramers.

far-field configurations at different resonant modes (near bright, Fano-like deep and dark resonant mode). The electric field distributions (especially the near field) show strong edge to edge interactions between NP_2 and NP_3, and NP_1 and NP_4 at different resonant modes (supplement S5). On the other hand, no visible edge to edge interaction is observed between NP_1 and NP_2, and NP_3 and NP_4 in the far-field configuration.

7. Effect of underneath background in far field and near field

Finally, we have demonstrated some similarities and differences between the far-field and near-field optical binding force characteristics when we increase the refractive index of the background medium. For both the far field and near field, we have used three different refractive index values (RI = 1.5, 1.7 and 2) of the background media. While comparing the effect of the underneath background in the optical binding force reversal, we have broken down this section into two different subsections: (i) similarity, and (ii) difference.

8. Similarity

The red shift of the resonant modes in both the far-field and near-field configurations is observed from the extinction spectra curves of figure 9. Reversal points of the face to face optical binding force also red shift due to high refractive index background medium. The dielectric screening factor $(\varepsilon_s - 1)/(\varepsilon_s + 1)$ induces a strong image charge in the background medium, and it leads to a strong interaction between the plasmon modes of the nanoparticles and the image charge. As a result, red shift of the resonant modes is observed in both the far field and near field. Also, a stable Fano-like resonance is observed for high refractive index background medium (a detailed discussion is given in the previous sections in figures 2 and 3), which leads to higher magnitude of the repulsive binding force. This observation leads to the idea of controllable Fano-like resonance and controllable face to face optical binding force reversal at different wavelengths. It shows how Fano-like resonance and the far- and near-field optical binding force reversal magnitude can be tuned by using different refractive index background medium. We have also observed that the red shift of

the bright resonant mode is greater than the dark resonant mode in both the far field and near field.

9. Difference

Figures 9(a)–(d) and (i)–(l) show a significant increase in the magnitude of the dark resonant mode in the near-field configuration compared to the far-field configuration due to the increase in the refractive index of the background medium. Also, figures 9(e)–(h) show a comparatively greater increase in the magnitude of the attractive binding force near the dark resonant mode in the near-field configuration compared to the far-field (figures 9(m)–(p)) configuration. The high refractive index medium induced high dielectric screening factor leads to a strong mixing of the dark resonant mode with the higher-order resonant modes. The dark resonant mode contains a significant mix with the higher-order modes compared to the bright resonant mode, which increases the net dipole moment near the dark resonant mode. In the near-field configuration, the mixing of the higher-order mode component is relatively greater due to small interparticle distance. As a result, the net dipole moment at the dark resonant mode arises more in the near-field configuration compared to the far field. High attractive binding forces at the near-field configuration (figures 9(e)–(h)) originate from the high magnitude of the induced dipole moment in the near-field configuration.

In our manuscript, for FDTD simulation, the incident intensity is mostly set as 0.001 176 W m^{-2}. The magnitude of the force is not scaled at a higher value considering this exact low value of input intensity in all the full-wave simulations. If we consider the incident intensity of light is 0.05×10^{12} W m^{-2} [which is commonly used in usual optical set-ups], the approximate magnitude of the optical binding force for our set-ups will be: $\frac{10^{-24}}{0.001\,176 \times 0.05 \times 10^{12}} \approx 42.52$ pN (in pico-Newton range [49, 69]). Therefore, we can safely conclude that the proposed results on optical binding forces can be experimentally verified for our set-ups, as these would be found in the pico-Newton range [49, 69] by properly adjusting/scaling the intensity of incident light beam.

10. Conclusion

In this work, we have proposed a specific symmetry breaking optical set-up, and have shown a robust, stable and controllable Fano-like plasmonic resonance for distinctly shaped (cube, cylinder, ring and sphere) plasmonic nanoclusters. This kind of Fano-like plasmonic resonance is even stable at interparticle distances more than 1 μm for different geometrical configurations. A comparative study on the far-field and near-field resonant modes (along with the optical binding force characteristics) has also been reported with a detailed analysis. We have illustrated the remarkable impact of the resonant modes on both the far-field and near-field optical binding forces in cube-, cylinder-, ring- and sphere-shaped tetramer set-ups. In our proposed optical set-up, the optical binding force and stable Fano-like resonance have been found for Mie-range objects; reversal of the optical binding force and such stable Fano-like plasmonic resonance have not been observed for the Rayleigh-range objects.

It is important to note that a clear connection between the far-field optical binding force and resonant modes (along with the Lorentz force dynamics) has been demonstrated in this work, which has not been reported previously in the literature. Here, we have shown that the Lorentz force is partially dependent on particle shape, where the Lorentz force dynamics in a sphere are quite different to those in a cube. In the meantime, we have also shown the unusual magnetic nature of the resonant modes in the far-field configuration, which is quite rare for such simple geometries, and it might further facilitate the study of negative refractive-index-based metamaterials.

In short, we have shown that background-dependent controllable Fano-like plasmonic resonance and binding force reversal (magnitude and reversal point) over wavelength can be achieved for distinctly shaped nanoparticles. These might open a novel way to develop resonant-mode-based chemical and biological sensors, and may also help in understanding the dynamics of particle aggregation, clustering, crystallization and self-assembly.

Acknowledgments

M R C Mahdy acknowledges the support of the internal grant of North South University 2018–19 and 2019–20 (approved by the members of BOT, North South University, Bangladesh) along with the support of a TWAS international grant 2018–19 (18-121 RG/PHYS/AS_I).

References

[1] Michaels A M, Jiang J and Brus L 2000 Ag nanocrystal junctions as the site for surface-enhanced Raman scattering of single rhodamine 6G molecules *J. Phys. Chem.* B **104** 11965

[2] Verellen N *et al* 2011 Plasmon line shaping using nanocrosses for high sensitivity localized surface plasmon resonance sensing *Nano Lett.* **11** 391–7

[3] Li K R, Stockman M I and Bergman D J 2003 Self-similar chain of metal nanospheres as an efficient nanolens *Phys. Rev. Lett.* **91** 227402

[4] Shegai T *et al* 2011 A bimetallic nanoantenna for directional colour routing *Nat. Comm.* **2** 481

[5] Fan J A, Wu C, Bao K, Bao J, Bardhan R, Halas N J, Manoharan V N, Nordlander P, Shvets G and Capasso F 2010 Self-assembled plasmonic nanoparticle clusters *Science* **328** 1135–8

[6] Hentschel M, Dregely D, Vogelgesang R, Giessen H and Liu N 2011 Plasmonic oligomers: the role of individual particles in collective behavior *ACS Nano* **5** 2042–50

[7] Fan J A, Bao K, Wu C, Bao J, Bardhan R, Halas N J, Manoharan V N, Shvets G, Nordlander P and Capasso F 2010 Fano-like interference in self-assembled plasmonic quadrumer clusters *Nano Lett.* **10** 4680–5

[8] Rahmani M, Lei D Y, Giannini V, Lukiyanchuk B, Ranjbar M, Liew T Y F, Hong M and Maier S A 2012 Subgroup decomposition of plasmonic resonances in hybrid oligomers: modeling the resonance lineshape *Nano Lett.* **6** 2101–6

[9] Dregely D, Hentschel M and Giessen H 2011 Excitation and tuning of higher-order Fano resonances in plasmonic oligomer clusters *ACS Nano* **5** 8202–11

[10] Mahdy M R C, Zhang T, Danesh M and Ding W 2017 Substrate and Fano resonance effects on the reversal of optical binding force between plasmonic cube dimers *Sci. Rep.* **7** 6938

[11] Burns M M, Fournier J-M and Golovchenko J A 1989 Optical binding *Phys. Rev. Lett.* **63** 1233

[12] Fazal F M and Block S M 2011 Optical tweezers study life under tension *Nat. Photon.* **5** 318–21

[13] Arthur A and Dziedzic J M 1987 Optical trapping and manipulation of viruses and bacteria *Science* **235** 1517–20

[14] Ashkin A 1970 Acceleration and trapping of particles by radiation pressure *Phys. Rev. Lett.* **24** 156–9

[15] Gao D, Ding W, Nieto-Vesperinas M, Ding M, Mahdy M R C, Zhang T, Lim C T and Qiu C W 2017 Optical manipulation from the microscale to the nanoscale: fundamentals, advances and prospects *Light: Sci., Article* **6** e17039

[16] Dienerowitz M, Mazilu M and Dholakia K 2008 Optical manipulation of nanoparticles: a review *J. Nanophotonics* **2** 021875

[17] Chan J, Alegre T M, Safavi-Naeini A H, Hill J T, Krause A, Gröblacher S and Painter O 2011 Laser cooling of a nanomechanical oscillator into its quantum ground state *Nature* **478** 89

[18] Neuman K C and Nagy A 2008 Single-molecule force spectroscopy: optical tweezers, magnetic tweezers and atomic force microscopy *Nat. Methods* **5** 491–505

[19] Burns M M, Fournier J-M and Golovchenko J A 1990 Optical matter: crystallization and binding in intense optical fields *Science* **249** 749–54

[20] Kumar M S, Andrews J T and Gupta P K 2004 Enhanced optical forces between coupled resonant metal nanoparticles *Opt. Express* **12** 2746–53

[21] Dholakia K and Zemánek P 2010 Colloquium: gripped by light: optical binding *Rev. Modern Phys.* **82** 1767

[22] Hallock A J, Redmond P L and Brus L E 2005 Optical forces between metallic particles *Proc. Natl Acad. Sci.* **102** 1280–4

[23] Rivy H M, Mahdy M R C, Jony Z R, Masud N, Satter S S and Jani R 2019 Plasmonic or dielectric dimers: a generic way to control the reversal of near field optical binding force *Opt. Commun.* **430** 51–62

[24] Dienerowitz M, Mazilu M, Reece P J, Krauss T F and Dholakia K 2008 Optical vortex trap for resonant confinement of metal nanoparticles *Opt. Express* **16** 4991–9

[25] Brzobohaty O, Cizmar T, Karasek V, Siler M, Dholakia K and Zemanek P 2010 Experimental and theoretical determination of optical binding forces *Opt. Express* **18** 25389–401

[26] Summers M D, Dear R D, Taylor J M and Ritchie G A D 2012 Directed assembly of optically bound matter *Opt. Express* **20** 1001–12

[27] Demergis V and Florin E L 2012 Ultrastrong optical binding of metallic nanoparticles *Nano Lett.* **12** 5756–60

[28] Bowman R W and Miles J P 2013 Optical trapping and binding *Rep. Progression. Phys.* **76** 026401

[29] Chaumet P C and Nieto-Vesperinas M 2001 Optical binding of particles with or without the presence of a flat dielectric surface *Phys. Rev.* B **64** 035422

[30] Grzegorczyk T M, Brandon A K and Kong J A 2006 Stable optical trapping based on optical binding forces *Phys. Rev. Lett.* **96** 113903

[31] Karasek V, Cizmar T, Brzobohaty O, Zemanek P, GarcesChavez V and Dholakia K 2008 Long-range one-dimensional longitudinal optical binding *Phys. Rev. Lett.* **101** 143601

[32] Zhang Q, Xiao J J, Zhang X M, Yao Y and Liu H 2013 Reversal of optical binding force by Fano resonance in plasmonic nanorod heterodimer *Opt. Express* **21** 6601–8

[33] Fan J A *et al* 2010 Self-assembled plasmonic nanoparticle clusters *Science* **328** 1135–8

[34] Miljkovic V D, Pakizeh T, Sepulveda B, Johansson P and Kall M 2010 Optical forces in plasmonic nanoparticle dimers *J. Phys. Chem.* C **114** 7472–9

[35] Liu H, Ng J, Wang S B, Hang Z H, Chan C T and Zhu S N 2011 Strong plasmon coupling between two gold nanospheres on a gold slab *New J. Phys.* **13** 073040

[36] Ng J, Tang R and Chan C T 2007 Electrodynamics study of plasmonic bonding and anti-bonding forces in a biosphere *Phys. Rev.* B **77** 195407

[37] Epasse F and Vigoureux J-M 1994 Optical binding force between two Rayleigh particles *J. Phys. D: Appl. Phys.* **27** 914–9

[38] Mahdy M R C, Danesh M, Zhang T, Ding W, Rivy H M, Chowdhury A B and Mehmood M Q 2018 Plasmonic spherical heterodimers: reversal of optical binding force based on the forced breaking of symmetry *Sci. Rep.* **8** 3164

[39] Rodriguez J, Davila Romero L C and Andrews D L 2008 Optical binding in nanoparticle assembly: potential energy landscapes *Phys. Rev.* A **78** 043805

[40] Zhang Q and Xiao J J 2013 Multiple reversals of optical binding force in plasmonic disk-ring nanostructures with dipole-multipole Fano resonances *Opt. Lett.* **38** 4240–3

[41] Palik E D 1998 *Handbook of Optical Constants of Solids* (Amsterdam: Elsevier)

[42] A commercial-grade simulator based on the finite-difference time-domain method was used to perform the calculations (https://lumerical.com/tcad-products/fdtd/) (accessed Jan 28, 2018)

[43] Circular polarization and phase convention | Lumerical Knowledge Base (https://kb.lumerical.com/en/ref_sim_obj_planewave_circular_polarization.html)

[44] Zhang T, Mahdy M R C, Liu Y, Teng J H, Lim C T, Wang Z and Qiu C W 2017 All-optical chirality-sensitive sorting via reversible lateral forces in interference fields *ACS Nano* **11** 4292–300

[45] Monzon C and Forester D W 2005 Negative refraction and focusing of circularly polarized waves in optically active media *Phys. Rev. Lett.* **95** 1–4

[46] Singh R, Plum E, Menzel C, Rockstuhl C, Zheludev N I and Zhang W 2011 Negative index in chiral metamaterials *IEEE Photonic Soc. 24th Annu. Meet. PHO* 240–1 23901 (January)

[47] Qiu C-W, Ding W, Mahdy M R C, Gao D, Zhang T, Cheong F C, Dogariu A, Wang Z and Lim C T 2015 Photon momentum transfer in inhomogeneous dielectric mixtures and induced tractor beams *Light: Sci. Appl.* **4** e278–278

[48] Zhu T, Mahdy M R C, Cao Y, Lv H, Sun F, Jiang Z and Ding W 2016 Optical pulling using evanescent mode in sub-wavelength channels *Opt. Express* **24** 18436

[49] Satter S S, Mahdy M R C, Ohi M A R, Islam F and Rivy H M 2018 Plasmonic cube tetramers over substrates: reversal of binding force as the effect of Fano resonance and light polarization *J. Phys. Chem.* C **122** 20923–34

[50] Volumetric Technique | Lumerical Knowledge Base (https://kb.lumerical.com/en/nanophotonic_applications_optical_tweezers_volumetric_technique.html) (accessed Mar 8 2018)

[51] Chaumet P C and Nieto-Vesperinas M 2000 Time-averaged total force on a dipolar sphere in an electromagnetic field *Opt. Lett.* **25** 1065–7

[52] Nieto-Vesperinas M, Sáenz J J, Gómez-Medina R and Chantada L 2010 Optical forces on small magnetodielectric particles *Opt. Express* **18** 11428–43

[53] Albaladejo S, Marqués M I, Laroche M and Sáenz J J 2009 Scattering forces from the curl of the spin angular momentum of a light field *Phys. Rev. Lett.* **11** 113602
[54] Zhou F, Wang C, Dong B, Chen X, Zhang Z and Sun C 2016 Scalable nanofabrication of U-shaped nanowire resonators with tunable optical magnetism *Opt. Express* **24** 6367–80
[55] Liu W, Miroshnichenko A E, Neshev D N and Kivshar Y S 2012 Polarization-independent Fano resonances in arrays of core-shell nanoparticles *Phys. Rev.* B **86** 081407
[56] Pinchuk A and Schatz G 2005 Anisotropic polarizability tensor of a dimer of nanospheres in the vicinity of a plane substrate *Nanotechnol.* **16** 2209–17
[57] Chen J, Ng J, Lin Z and Chan C T 2011 Optical pulling force *Nat. Photonics* **5** 531
[58] Limonov M F, Rybin M V, Poddubny A N and Kivshar Y S 2017 Fano resonances in photonics *Nat. Photonics* **11** 543
[59] Shorokhov A S, Melik-Gaykazyan E V, Smirnova D A, Hopkins B, Chong K E, Choi D Y and Kivshar Y S 2016 Multifold enhancement of third-harmonic generation in dielectric nanoparticles driven by magnetic Fano resonances *Nano Lett.* **16** 4857–61
[60] Miroshnichenko A E and Kivshar Y S 2012 Fano resonances in all-dielectric oligomers *Nano Lett.* **12** 6459–63
[61] Pinchuk A, Hilger A, Von Plessen G and Kreibig U 2004 Substrate effect on the optical response of silver nanoparticles *Nanotechnol.* **15** 1890–6
[62] Zhao R, Tassin P, Koschny T and Soukoulis C M 2010 Optical forces in nanowire pairs and metamaterials *Opt. Express* **18** 25665
[63] Shafiei F, Monticone F, Le Q, Liu K, Liu X, Hartsfield T, Alù A and Li X 2013 A subwavelength plasmonic metamolecule exhibiting magnetic-based optical Fano resonance *Nat. Nanotechnol.* **8** 95–9
[64] Cherqui C *et al* 2016 STEM/EELS imaging of magnetic hybridization in symmetric and symmetry-broken plasmon oligomer dimers and all-magnetic Fano interference *Nano Lett.* **16** 6668–76
[65] Campione S, Warne L K and Basilio I L 2017 Dipole approximation to predict the resonances of dimers composed of dielectric resonators for directional emission *Radio Sci.* **52**
[66] Mousavi S H, Khanikaev A B and Allen J 2015 Monica allen, and gennady shvets. Gyromagnetically induced transparency of metasurfaces *Phys. Rev. Lett.* **112** 117402
[67] Liu B, Tang E, Chen J, Yan Z, Zhu M, Sui Y and Tang H 2017 The coupling effects of surface plasmon polaritons and magnetic dipole resonances in metamaterials *Nanoscale Res. Lett.* **12** 586
[68] Wu P C, Hsu W-L, Chen W T, Huang Y-W, Liao C Y, Liu A Q, Zheludev N I, Sun G and Tsai D P 2015 Plasmon coupling in vertical split-ring resonator metamolecules *Sci. Rep.* **5** 9726
[69] Ng J, Tang R and Chan C T 2008 Electrodynamics study of plasmonic bonding and anti-bonding forces in a bisphere *Phys. Revi.* B **77** 195407